

Evaluation of Morphodynamic Controls on the Preservation of Fluvial Meander-belt Deposits

Na Yan¹, Luca Colombera¹, and Nigel P Mountney¹

¹University of Leeds

November 22, 2022

Abstract

The way river morphodynamics influence the preservation of point-bar deposits at different spatio-temporal scales is hitherto unquantified. Employing time-lapse trajectories of natural rivers, a numerical model is used here to simulate planform evolutions of meander-belt reaches that embody different transformation behaviors and cutoff processes. Proxies for temporal durations are obtained considering the surface area over which a river migrated and channel migration rates that relate to average channel radius of curvature through constant, monotonic and non-monotonic relationships. The preservation of meander-belt deposits over different timescales is assessed at three architectural hierarchies: (i) pairs and (ii) sets of accretion packages, and (iii) meander-belts. Results show that sediment preservation decreases in a predictable way with the accumulation time; however, accretion rates decay with time in a way that does not follow the expected power-law. This is interpreted to reflect the effect of the onset of geomorphic thresholds of channel transformation and cutoff.

1 **Evaluation of Morphodynamic Controls on the Preservation of Fluvial Meander-belt**
2 **Deposits**

3 **N. Yan¹, L. Colombera¹, and N. P. Mountney¹**

4 ¹Fluvial, Eolian & Shallow-Marine Research Group, School of Earth and Environment,
5 University of Leeds, Leeds, LS2 9JT, United Kingdom.

6 Corresponding author: Na Yan (n.yan@leeds.ac.uk)

7 **Key Points:**

- 8 • The preservation of meander-belt deposits is assessed at multiple scales through
9 numerical simulations of river migration histories.
- 10 • Accretion rates of fluvial meander belts decay with time in a way that does not regularly
11 follow a simple power-law relationship.
- 12 • Geomorphic thresholds of meander-transformation change and bend cutoff likely account
13 for nonlinearity in stratigraphic completeness.

14 **Abstract**

15 The way river morphodynamics influence the preservation of point-bar deposits at different
16 spatio-temporal scales is hitherto unquantified. Employing time-lapse trajectories of natural
17 rivers, a numerical model is used here to simulate planform evolutions of meander-belt reaches
18 that embody different transformation behaviors and cutoff processes. Proxies for temporal
19 durations are obtained considering the surface area over which a river migrated and channel
20 migration rates that relate to average channel radius of curvature through constant, monotonic
21 and non-monotonic relationships. The preservation of meander-belt deposits over different
22 timescales is assessed at three architectural hierarchies: (i) pairs and (ii) sets of accretion
23 packages, and (iii) meander-belts. Results show that sediment preservation decreases in a
24 predictable way with the accumulation time; however, accretion rates decay with time in a way
25 that does not follow the expected power-law. This is interpreted to reflect the effect of the onset
26 of geomorphic thresholds of channel transformation and cutoff.

27 **Plain Language Summary**

28 Larger sediment volumes tend to record slower rates of deposition, because the likelihood of
29 incorporating significant gaps in sedimentation increases with time. Hence, over timescales from
30 seconds to millions of years, accumulation rates decrease as a power of time. This research
31 determines whether this relationship holds true for channel belts produced by meandering rivers,
32 and in particular for deposits that may develop over timescales of days (beds in point bars) to
33 millennia (meander belts consisting of amalgams of bars and abandoned channels). To do this, a
34 numerical model is applied to reconstruct the planform evolution of natural rivers. This way,
35 sedimentation, erosion, and sediment preservation can be quantified, and proxies for time can be
36 established based on the area over which a river migrated. The results show that, over this time
37 window, the dependency of accumulation rates with time is more complex than anticipated. This
38 is likely due, in part, to the sudden onset of changes in the style of river evolution (e.g., from
39 meanders swinging laterally to sweeping downstream) and of bend cutoffs, which drive
40 significant erosional reworking.

41 **1 Introduction**

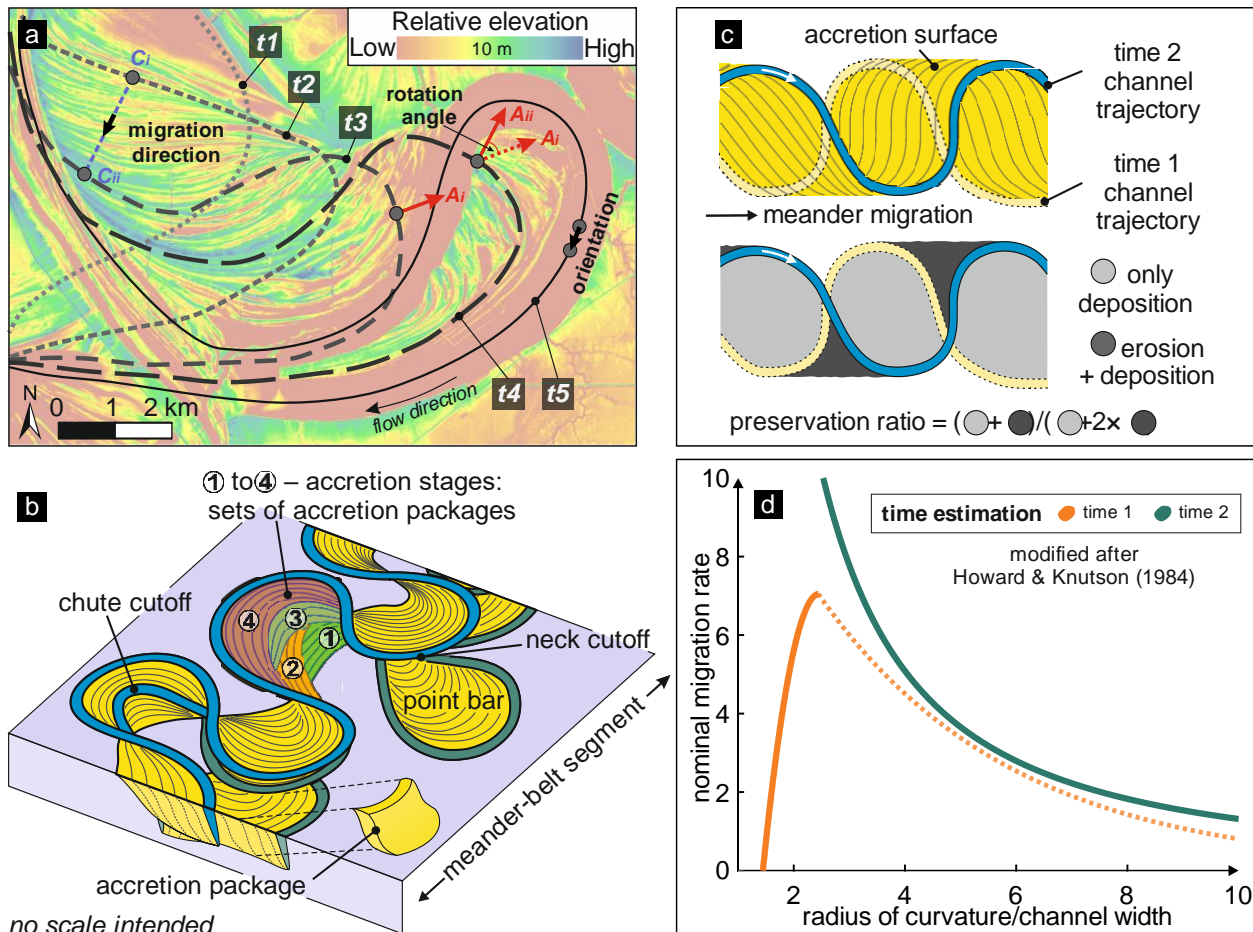
42 Sediment accumulation rates tend to decrease with the time span over which they are
43 determined: the so-called ‘Sadler effect’ (Sadler, 1981; Sadler and Strauss, 1990). This happens
44 because depositional processes are episodic in nature, and the average length of time gaps at any
45 point in space tends to increase with the time window considered (Ager, 1993; Barrell, 1917;
46 Dott Jr, 1996; Miall, 2015). The fraction of time recorded in a stratigraphic section
47 (‘stratigraphic completeness’) is therefore itself dependent on time (Sadler and Strauss, 1990).
48 Based on analysis of natural examples and numerical modeling, Durkin et al. (2018) quantified
49 the stratigraphic completeness of fluvial meander-belt deposits, demonstrating how sediment
50 preservation follows a natural logarithmic decay with time. Yet, the preservation of channel-belt
51 sediments is expected to vary significantly in relation to the natural variability of river
52 morphodynamics. Fluvial meanders can evolve through multiple stages of bar growth, each of
53 which may be dominated by different bend-transformation behaviors: lateral expansion vs.
54 downstream translation, commonly in combination with bend-apex rotation (Daniel, 1971;
55 Hagstrom et al., 2019). Previously accumulated point-bar deposits can undergo partial erosion,
56 leading to the formation of potentially complex mosaics of accretion patterns (Durkin et al.,
57 2015; Johnston and Holbrook, 2019; Strick et al., 2018; Willis and Sech, 2019). The amount of

58 intra-channel-belt erosion depends critically on meander-transformation behavior (Durkin et al.,
59 2018; Ghinassi et al., 2016). Over longer timescales, meander cut-offs can lead to the
60 abandonment of point-bar deposits; these can later be subject to cannibalization by the mobile
61 river (Constantine and Dunne, 2008). The stratigraphic completeness of meander-belt deposits is
62 related to all these processes. However, whether these mechanisms lead to a classic Sadler effect,
63 whereby a power-law relationship exists between accretion rates and measurement intervals
64 (Sadler, 1981), has yet to be determined. This is rendered difficult by the limited availability of
65 meander-belt examples for which a detailed temporal framework exists, since historical maps
66 and radiocarbon or OSL dating, for example, can only provide spot measurements. In this work
67 we aim to address this gap by applying a numerical model to the simulation of idealized river
68 systems that display planform evolutions like those seen in nature.

69 **2 Methodology**

70 The Point-Bar Sedimentary Architecture Numerical Deduction (PB-SAND; Yan et al.,
71 2017) is a numerical model that simulates the planform evolution of meander belts based on
72 input consisting of centerlines representing the river course at selected time steps (Figure 1a). In
73 PB-SAND, channel evolution and resulting channel-belt accretion and erosion are modeled by
74 linear interpolation between input river trajectories (Yan et al., 2017, 2020a, b). Thirty-four
75 idealized meander-belt reaches that vary in bend-transformation styles and number of channel
76 cut-off events are modeled based on planform evolutions documented in accretion patterns of
77 natural analogs, visible in satellite images, LiDAR topographies or historical maps (Figure S1 in
78 Supplementary Material). The idealized river planforms are normalized such that the formative-
79 channel width is the same across all examples. The tempo of point-bar accretion is dictated by
80 the chosen spacing of accretion surfaces to mimic scroll-bar morphologies observed in nature. In
81 the model outputs, three depositional hierarchies are considered for analysis (Figure 1b): (i) pairs
82 of accretion packages, wherein each package is contained between two consecutive accretion
83 surfaces; individual accretion packages are not considered because erosion within them is not
84 simulated; (ii) sets of accretion packages (here termed ‘accretion stages’) bounded by two
85 consecutive input trajectories, representing phases of point-bar growth with a given style of
86 meander transformation; and (iii) meander-belt segments that are composed of multiple sets of
87 accretion packages, each of which may be dominated by different styles of meander
88 transformation. Accretion packages can be regarded as analogous to flood-interflood units. Due
89 to their generation by linear interpolation between input trajectories, accretion packages in each
90 stage exhibit similar amounts of accretion (see Supplementary Material).

91



92 no scale intended

93 **Figure 1.** Illustration of methods. (a) Example input trajectories digitized over a LiDAR
 94 topography; t_1 to t_5 denote chronological order. ‘C’ and ‘A’ denote a control point and a meander
 95 apex, respectively. (b) hierarchies of sedimentary architecture considered here: accretion
 96 packages, accretion stages and meander-belt segments. (c) Definition of sediment preservation
 97 ratio. (d) Relationships between nominal channel migration rate and channel radius of curvature
 98 normalized by channel width (Howard and Knutson, 1984), used to estimate times of channel
 99 migration; migration rates are on arbitrary scale.

100 The ‘preservation ratio’ is the fraction of meander-belt deposits that are preserved over a
 101 given timescale, quantified as the ratio between the planform area covered by deposits
 102 accumulated over a certain time that are preserved (area of net deposition) and the area over
 103 which the river has wandered over the same time (area of river migration) (Durkin et al., 2018)
 104 (Figure 1c). The time recorded in each accretion package is determined by the ratio between
 105 channel migration distance and channel migration rate. The channel migration distance is
 106 determined by the ratio between the surface area subtended by two centerlines and their average
 107 length. Values of average channel migration rate over each depositional package (i.e. between
 108 two consecutive channel centerlines) are determined separately based on three different
 109 assumptions of its relationship with the channel radius of curvature (Howard and Knutson, 1984;
 110 Hudson and Kesel, 2000; Nanson and Hickin, 1983; Sylvester et al., 2019): (i) constant channel
 111 migration rate for any value of channel radius of curvature; (ii) migration rate increasing
 112 monotonically as the channel radius of curvature decreases (i.e. channel curvature increases);

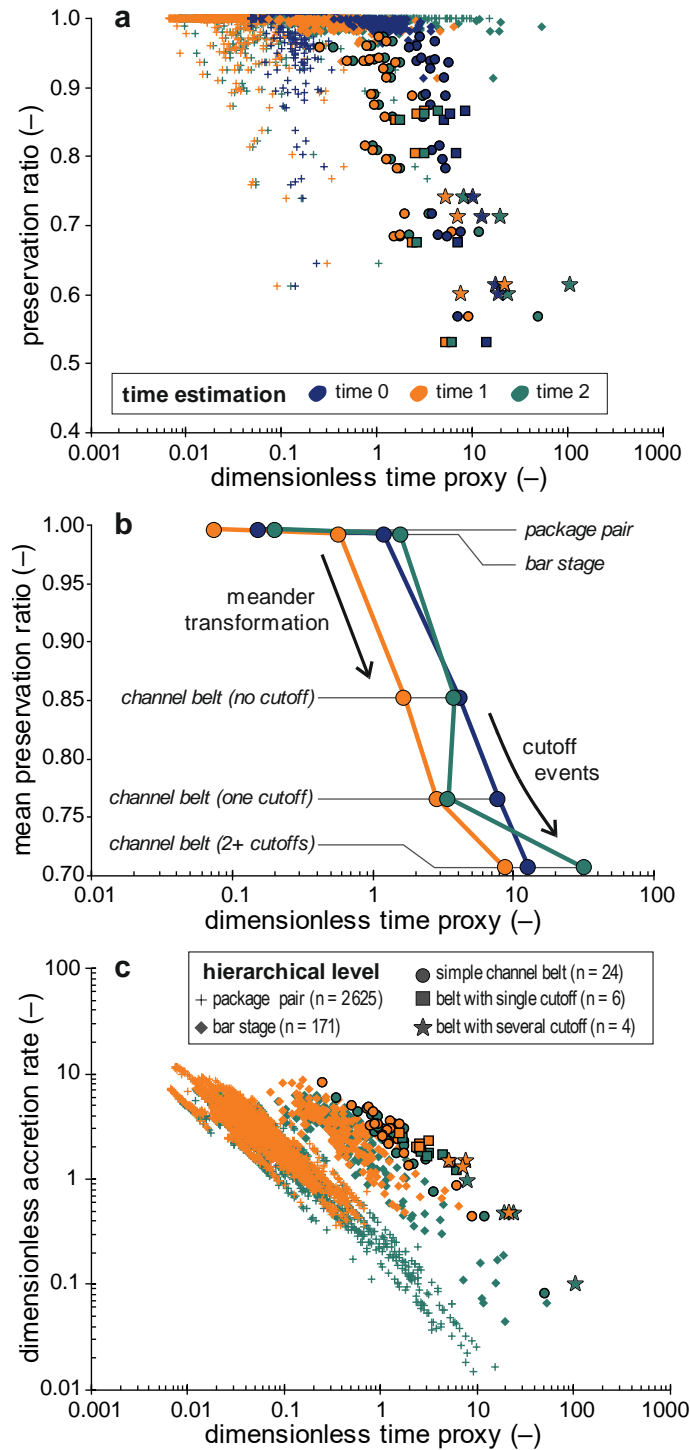
113 (iii) migration rate increasing as the ratio of radius of curvature to channel width decreases
114 towards a value of 2.44 (Howard and Knutson, 1984), and then decreasing as the radii of
115 curvature decrease further. The second and third alternatives are determined based on
116 relationships between channel radius of curvature and nominal migration rates that return
117 realistic relationships between actual channel migration rates and channel curvature in models by
118 Howard and Knutson (1984). For these relationships (Figure 1d), the dimensionless arbitrary
119 scale of Howard and Knutson (1984) is maintained. The dimensionless accretion time is
120 determined by the ratio of migration distance to average migration rate. The two proxies for time
121 length associated with the second and third alternatives ('time 1' and 'time 2' hereafter) are also
122 employed to compute meander-belt accretion rates, the ratio between accretion distance and
123 dimensionless time.

124 Planform characteristics of each architectural hierarchy are characterized in terms of
125 average circular variance of channel centerlines, meander-apex rotation, and accretion style
126 (Figure 1a). The circular variance of channel orientation is computed along the downstream
127 direction for pairs of consecutive control points (centerlines vector nodes); this is an indirect
128 measure of channel sinuosity. A quantity called 'migration angle' is defined for each accretion
129 package as the absolute angle between the direction of channel migration – approximated by the
130 direction of shift of corresponding control points across two consecutive trajectories – and the
131 circular mean of downstream channel direction, which approximates the channel-belt orientation
132 (Figure 1a). The degree of rotation of meanders is defined as the change of direction of the
133 meander apex, itself identified as the point of local maximum curvature between two channel
134 inflection points, across consecutive accretion packages (Figure 1a). The degree of rotation for
135 each meander belt is the average across all meanders. A more detailed description of the methods
136 is provided in the Supplementary Material.

137 **3 Results**

138 For each architectural hierarchy, the sediment preservation ratio decreases overall as the
139 time span of sedimentation increases, in a similar manner across the three approaches used to
140 estimate time (Figures 2a & b). The variability in preservation ratio is limited for package pairs
141 (st. dev. = 0.019, mean = 0.997) and accretion stages (st. dev. = 0.010, mean = 0.993) (Figure
142 S5), but more significant for meander-belt segments (st. dev. = 0.128, mean = 0.816). A
143 systematic decrease in preservation with channel-belt maturity (Figure 2b) reflects the combined
144 effect of intra-point-bar erosion between accretion stages and point-bar cannibalization following
145 bend cut-offs. The average preservation ratio is 0.84, 0.77 and 0.67, for meander belts that
146 respectively record no cut-off (N=24), a single cut-off (N=6), and multiple cut-off events (N=4).

147



148

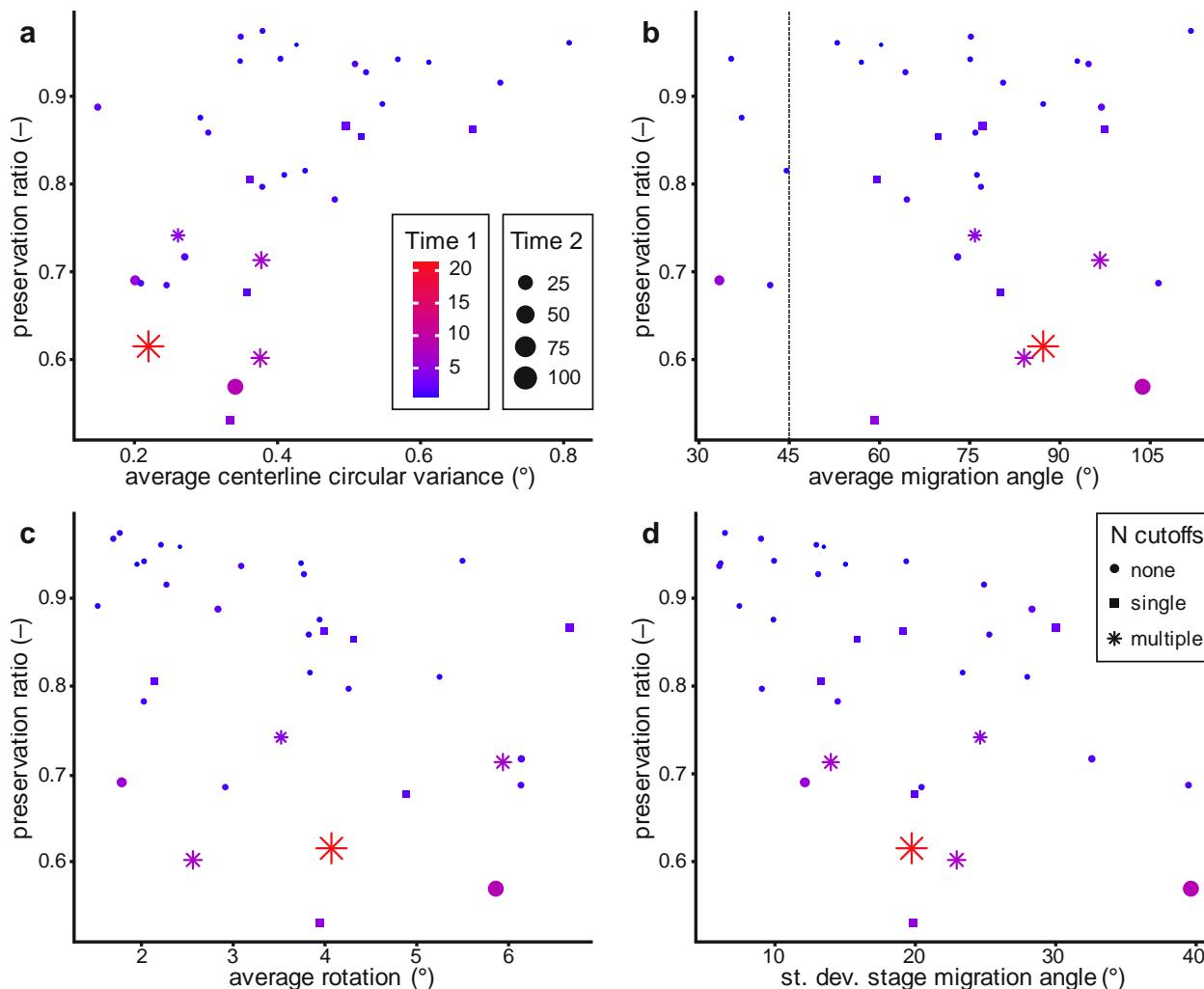
149 **Figure 2.** Scatterplots of preservation ratio (a), mean preservation ratio (b) and accretion rate (c)
 150 vs time span, for the different architectural hierarchies and approaches to time estimation.

151 Negative power-laws emerge between accretion rates and both ‘time 1’ and ‘time 2’, with
 152 coefficients of determination (R^2) of 0.56 and 0.71, and with exponents of -0.44 and -0.60,
 153 respectively. These exponents differ markedly from the value of -0.75 documented by Sadler
 154 (1981; Pelletier and Turcotte, 1997) (Figure 2c). Stronger power-laws can also be fitted to each

155 architectural hierarchy for both computed times, with R2 varying between 0.73 and 0.93, and
156 exponents ranging from -0.61 to -0.80.

157 Sediment preservation ratios tend to covary with meander-belt planform characteristics
158 (Figure 3). Meander belts with lower average centerline circular variance tend to have lower
159 preservation ratio (Figure 3a). This may reflect (i) how downstream bend translation tends to
160 maintain channel sinuosity while driving point-bar erosion by sweeping meanders, at a shorter
161 timescale (Ghinassi et al., 2016), and (ii) how periodic cutoffs reduce channel sinuosity while
162 causing point-bar cannibalization, at a longer timescale (Camporeale et al., 2008). The average
163 migration angle does not show correlation with the preservation ratio (Figure 3b), possibly
164 because this quantity can fail to capture the type of bend transformation (Yan et al., 2020b), but
165 also because of a lack of examples that record long-term channel evolutions dominated by bend
166 translation. The average bend rotation correlates weakly with the preservation ratio for cases of
167 comparable timescales (Figure 3b). However, the data suggest that the effect of rotation as a
168 mechanism of intra-point bar erosion on sediment preservation may be subordinate. Modest
169 correlation exists between the standard deviation of migration angles across accretion stages and
170 the preservation ratio (Figure 3d). This may reflect the effect of toggling between expansion and
171 translation on intra-point bar erosion (cf. Johnston and Holbrook, 2019).

172



173

174 **Figure 3.** Scatterplots of preservation ratio vs metrics describing planform characteristics of
 175 meander belts, for two different approaches to time estimation.

176 **4 Discussion**

177 The adopted numerical modeling approach allows simulation of meander-belt evolutions
 178 that are inherently realistic, being based on natural examples. Yet it also permits a systematic
 179 evaluation of sediment preservation over a range of timescales and at a resolution that would not
 180 be achievable using datasets from rivers for which chronometric constraints are available.
 181 Results from the numerical models elucidate how sediment preservation is determined by
 182 morphodynamic processes that operate at different spatial and temporal scales, and that affect
 183 depositional units of variable hierarchies. It therefore becomes possible to determine whether and
 184 where the so-called ‘Sadler effect’ – the dependency of sediment accumulation rate on timescale
 185 (Bailey and Smith, 2005; Durkin et al., 2018; Holbrook and Miall, 2020; Miall, 2015; Plotnick,
 186 1986; Sadler, 1981, 1999) – persists or breaks down in meander-belt successions, when
 187 considered for datasets with suitable continuity and granularity in the record of processes and
 188 products. It is significant that a single power-law relationship between time and point-bar
 189 accretion rate that would align with the power law observed for fluvial deposits *tout court*
 190 (Pelletier and Turcotte, 1997; Sadler, 1981) does not emerge. Instead, the three architectural

191 hierarchies, associated with different timescales, appear to yield different power-law
192 relationships. Important overlap exists in the preservation ratio and the accretion rate of package
193 pairs and stages (Figure 2c). This likely reflects how the rate of erosion of developing point bars
194 remains relatively steady in time under conditions of constant style of meander transformation;
195 this situation may be best depicted by meanders undergoing progressive bend tightening. When
196 changes of meander transformation styles occur, instead, more significant intra-point-bar erosion
197 commonly takes place (Durkin et al., 2018; Hagstrom et al., 2019; Johnston and Holbrook,
198 2019). Significant erosion can occur when formerly expansional meanders commence a
199 trajectory of downstream migration, for example where channel banks encounter less erodible
200 substrates, such as valley walls or abandoned channel fills (Ghinassi et al., 2016). Meander
201 rotation is also a driver of point-bar erosion, especially in the vicinity of the outer banks of
202 rotating apices (Ielpi and Ghinassi, 2014; Strick et al., 2018). Yet, the role of steady meander
203 rotation in generating intra-point-bar erosion may be secondary relative to threshold changes
204 from one meander transformation style to another (Figure 3), since such erosion tends to be
205 localized (Yan et al., 2020b). The influence of neck or chute cutoff events on the long-term
206 preservation of channel-belt deposits only becomes important for channel belts that have reached
207 a certain maturity. Cutoffs serve as a geomorphic threshold that drives the systematic obliteration
208 of older reaches (Camporeale et al., 2008; Schumm, 1973) and that potentially triggers further
209 cutoff and ensuing channel-belt erosion (Schwenk and Fofoula-Georgiou, 2016).

210 The modelling approach taken in this work is subject to limitations (see Supplementary
211 Material). The assessment of sediment preservation of meander belts was undertaken considering
212 planform areas as proxies for sediment volumes (Durkin et al., 2018), therefore disregarding
213 changes in meander-belt thickness and aggradation on preserved volumes. The influence of
214 autogenic dynamics (e.g., bend cutoff; Schwenk and Fofoula-Georgiou, 2016) on accretion
215 rates, and hence recorded time, is also not considered. The time embodied by accretion packages
216 was calculated based on trajectories that are linearly interpolated, effectively assuming that
217 point-bar accretion in each stage takes place in regular pulses (meaning that 10-year or 100-year
218 floods, for example, are assumed to have comparable impacts), and that hiatuses of variable
219 magnitude associated with accretion surfaces do not exist. In reality, the amount of erosion
220 recorded between and within individual accretion packages can be considerable (cf. Moody and
221 Meade, 2014), but the fragmentary nature of point-bar bedsets is not simulated through the
222 chosen approach. This is likely to explain, at least in part, the limited variability in preservation
223 between accretion-package pairs and stages.

224 **5 Conclusions**

225 Detailed reconstructions of meander-belt evolutions have revealed the role of different
226 morphodynamic processes in controlling point-bar sediment preservation over a range of
227 timescales. In the channel belts of meandering river systems, relationships between time,
228 preservation and accretion rates appear to be rendered complicated by threshold processes of
229 meander transformation change and bend cutoff. Yet, nonlinearity in point-bar accretion cannot
230 be captured by a simple power law between sedimentation rate and time. This has implications
231 for the inference of the temporal significance of depositional units of variable hierarchy.

232

233 **Acknowledgments**

234 We thank CNOOC International, Canada (formerly Nexen), for financial support for
 235 development of PB-SAND, and FRG-ERG-SMRG sponsors (AkerBP, Areva [now Orano], BHP,
 236 Cairn India [Vedanta], Chevron, CNOOC International, ConocoPhillips, Equinor, Murphy Oil,
 237 Occidental, Saudi Aramco, Shell, Tullow Oil, Woodside and YPF) and our partner
 238 Petrotechnical Data Systems for financial support of the research group.

239 **Data Availability Statement**

240 Data of this study are available from the data repository of the University of Leeds at
 241 <https://doi.org/10.5518/970>.

242 **References**

- 243 Ager, D. V. (1993). *The nature of the stratigraphical record*. Chichester: John Wiley & Sons.
- 244 Bailey, R. J., & Smith, D. G. (2005). Quantitative evidence for the fractal nature of the
 245 stratigraphic record: Results and implications. *Proceedings of the Geologists'*
 246 *Association*, 116(2), 129-138. [https://doi.org/10.1016/S0016-7878\(05\)80004-5](https://doi.org/10.1016/S0016-7878(05)80004-5)
- 247 Barrell, J. (1917). Rhythms and the measurements of geologic time. *Bulletin of the Geological*
 248 *Society of America*, 28(1), 745-904. <https://doi.org/10.1130/GSAB-28-745>
- 249 Camporeale, C., Perucca, E., & Ridolfi, L. (2008). Significance of cutoff in meandering river
 250 dynamics. *Journal of Geophysical Research: Earth Surface*, 113(F1).
 251 <https://doi.org/10.1029/2006JF000694>
- 252 Constantine, J. A., & Dunne, T. (2008). Meander cutoff and the controls on the production of
 253 oxbow lakes. *Geology*, 36(1), 23-26. <https://doi.org/10.1130/G24130A.1>
- 254 Daniel, J. F. (1971). Channel movement of meandering Indiana streams. *US Geological Survey*
 255 *Professional Paper* 732-A.
- 256 Davies, N. S., Shillito, A. P., & McMahon, W. J. (2019). Where does the time go? Assessing the
 257 chronostratigraphic fidelity of sedimentary geological outcrops in the Pliocene–
 258 Pleistocene Red Crag Formation, eastern England. *Journal of the Geological Society*,
 259 176(6), 1154-1168. <https://doi.org/10.1144/jgs2019-056>
- 260 Dott Jr, R. (1996). Episodic event deposits versus stratigraphic sequences—shall the twain never
 261 meet? *Sedimentary Geology*, 104(1-4), 243-247. [https://doi.org/10.1016/0037-](https://doi.org/10.1016/0037-0738(95)00131-X)
 262 [0738\(95\)00131-X](https://doi.org/10.1016/0037-0738(95)00131-X)
- 263 Durkin, P. R., Hubbard, S. M., Boyd, R. L., & Leckie, D. A. (2015). Stratigraphic expression of
 264 intra-point-bar erosion and rotation. *Journal of Sedimentary Research*, 85(10), 1238-
 265 1257. <https://doi.org/10.2110/jsr.2015.78>
- 266 Durkin, P. R., Hubbard, S. M., Holbrook, J., & Boyd, R. (2018). Evolution of fluvial meander-
 267 belt deposits and implications for the completeness of the stratigraphic record. *GSA*
 268 *Bulletin*, 130(5-6), 721-739. <https://doi.org/10.1130/B31699.1>
- 269 Ghinassi, M., Ielpi, A., Aldinucci, M., & Fustic, M. (2016). Downstream-migrating fluvial point
 270 bars in the rock record. *Sedimentary Geology*, 334, 66-96.
 271 <https://doi.org/10.1016/j.sedgeo.2016.01.005>

- 272 Hagstrom, C. A., Hubbard, S. M., Leckie, D. A., & Durkin, P. R. (2019). The effects of
273 accretion-package geometry on lithofacies distribution in point-bar deposits. *Journal of*
274 *Sedimentary Research*, 89(5), 381-398. <https://doi.org/10.2110/jsr.2019.23>
- 275 Holbrook, J., & Miall, A. D. (2020). Time in the rock: a field guide to interpreting past events
276 and processes from a fragmentary siliciclastic archive. *Earth-Science Reviews*, 203,
277 103121. <https://doi.org/10.1016/j.earscirev.2020.103121>
- 278 Howard, A. D., & Knutson, T. R. (1984). Sufficient conditions for river meandering: A
279 simulation approach. *Water Resources Research*, 20(11), 1659-1667.
280 <https://doi.org/10.1029/WR020i011p01659>
- 281 Hudson, P. F., & Kesel, R. H. (2000). Channel migration and meander-bend curvature in the
282 lower Mississippi River prior to major human modification. *Geology*, 28(6), 531-534.
- 283 Ielpi, A., & Ghinassi, M. (2014). Planform architecture, stratigraphic signature and
284 morphodynamics of an exhumed Jurassic meander plain (Scalby Formation, Yorkshire,
285 UK). *Sedimentology*, v. 61(7), 1923-1960. [https://doi.org/10.1130/0091-](https://doi.org/10.1130/0091-7613(2000)28<531:CMAMCI>2.0.CO;2)
286 [7613\(2000\)28<531:CMAMCI>2.0.CO;2](https://doi.org/10.1130/0091-7613(2000)28<531:CMAMCI>2.0.CO;2)
- 287 Johnston, S., & Holbrook, J. (2019). Toggling between expansion and translation: The
288 generation of a muddy-normal point bar with an earthquake imprint. In M. Ghinassi, L.
289 Colombera, N. P. Mountney, & A. J. Reesink (Eds.), *Fluvial meanders and their*
290 *sedimentary products in the rock record. International Association of Sedimentologists*
291 *Special Publication*, 48, 47-80. <https://doi.org/10.1002/9781119424437.ch3>
- 292 Miall, A. D. (1996). *The Geology of Fluvial Deposits*. New York: Springer-Verlag.
- 293 Miall, A. D. (2015). Updating uniformitarianism: stratigraphy as just a set of ‘frozen accidents’.
294 In D. G. Smith, R. J. Bailey, P. M. Burgess, & A. J. Fraser (Eds.), *Strata and Time:*
295 *Probing the Gaps in Our Understanding*, Geological Society, London, *Special*
296 *Publications*, 404, 11-36. <https://doi.org/10.1144/SP404.4>
- 297 Moody, J. A., & Meade, R. H. (2014). Ontogeny of point bars on a river in a cold semi-arid
298 climate. *Geological Society of America Bulletin*, 126(9-10), 1301-1316.
299 <https://doi.org/10.1130/B30992.1>
- 300 Nanson, G. C., & Hickin, E. J. (1983). Channel Migration and Incision on the Beatton River.
301 *Journal of Hydraulic Engineering*, 109(3), 327-337.
302 [https://doi.org/10.1061/\(ASCE\)0733-9429\(1983\)109:3\(327\)](https://doi.org/10.1061/(ASCE)0733-9429(1983)109:3(327))
- 303 Pelletier, J. D., & Turcotte, D. L. (1997). Synthetic stratigraphy with a stochastic diffusion model
304 of fluvial sedimentation. *Journal of Sedimentary Research*, 67(6), 1060-1067.
305 <https://doi.org/10.1306/D42686C6-2B26-11D7-8648000102C1865D>
- 306 Plotnick, R. E. (1986). A fractal model for the distribution of stratigraphic hiatuses. *The Journal*
307 *of Geology*, 94(6), 885-890. <https://doi.org/10.1086/629094>
- 308 Sadler, P. M. (1981). Sediment accumulation rates and the completeness of stratigraphic
309 sections. *The Journal of Geology*, 89(5), 569-584. <https://www.jstor.org/stable/30062397>
- 310 Sadler, P. M. (1999). The influence of hiatuses on sediment accumulation rates. *Proceedings*
311 *GeoResearch Forum*, 5, 15-40.

- 312 Sadler, P. M., & Strauss, D. J. (1990). Estimation of completeness of stratigraphical sections
 313 using empirical data and theoretical models. *Journal of the Geological Society*, 147(3),
 314 471-485. <https://doi.org/10.1144/gsjgs.147.3.0471>
- 315 Schumm, S. (1973). Geomorphic thresholds and complex response of drainage systems. In M.
 316 Morisawa, M. (Ed.), *Fluvial Geomorphology*, Publications of Geomorphology, State
 317 University of New York, Binghamton, 299-310.
- 318 Schwenk, J., & Fofoula-Georgiou, E. (2016). Meander cutoffs nonlocally accelerate upstream
 319 and downstream migration and channel widening. *Geophysical Research Letters*, 43(24),
 320 12437-12445. <https://doi.org/10.1002/2016GL071670>
- 321 Strick, R. J. P., Ashworth, P. J., Awcock, G., & Lewin, J. (2018). Morphology and spacing of
 322 river meander scrolls. *Geomorphology*, 310, 57-68.
 323 <https://doi.org/10.1016/j.geomorph.2018.03.005>
- 324 Sylvester, Z., Durkin, P., & Covault, J. A. (2019). High curvatures drive river meandering.
 325 *Geology*, 47(3), 263-266. <https://doi.org/10.1130/G45608.1>
- 326 Willis, B. J., & Sech, R. P. (2019). Emergent facies patterns within fluvial channel belts. In M.
 327 Ghinassi, L. Colombera, N. P. Mountney, & A. J. Reesink (Eds.), *Fluvial meanders and*
 328 *their sedimentary products in the rock record. International Association of*
 329 *Sedimentologists Special Publication*, 48, 509-542.
- 330 Yan, N., Colombera, L., & Mountney, N. P. (2020a). Three-dimensional forward stratigraphic
 331 modelling of the sedimentary architecture of meandering-river successions in evolving
 332 half-graben rift basins. *Basin Research*, 32(1), 68-90. <https://doi.org/10.1111/bre.12367>
- 333 Yan, N., Colombera, L., & Mountney, N. P. (2020b). Controls on fluvial meander-belt thickness
 334 and sand distribution: Insights from forward stratigraphic modelling. *Sedimentology*.
 335 <https://doi.org/10.1111/sed.12830>
- 336 Yan, N., Mountney, N. P., Colombera, L., & Dorrell, R. M. (2017). A 3D forward stratigraphic
 337 model of fluvial meander-bend evolution for prediction of point-bar lithofacies
 338 architecture. *Computers & Geosciences*, 105, 65-80.
 339 <https://doi.org/10.1016/j.cageo.2017.04.012>

Geophysical Research Letters

Supporting Information for

Evaluation of Morphodynamic Controls on the Preservation of Fluvial Meander-belt Deposits

N. Yan¹, L. Colombera¹, and N. P. Mountney¹

¹Fluvial, Eolian & Shallow-Marine Research Group, School of Earth and Environment, University of Leeds, Leeds, LS2 9JT, United Kingdom.

Contents of this file

Text S1 (including Figures S1 to S4, and Table S1)
Figure S5

Introduction

This document provides a detailed description of methodology and additional supporting figures.

Text S1. Methodology

Thirty-four modern and recent natural meander-belt examples were selected for use in this study. These examples are representative of a range of meander transformation styles, record different degrees of bend-apex rotation, and incorporate a variable number of neck or chute cutoffs (Figure S1 and Table S1). The same types of planform morphodynamic evolutions seen in these meander belts were modeled by PB-SAND in application to idealized scale-free simulations. The real-world natural examples were employed to derive channel trajectories that track the temporal evolution of the rivers. The channel trajectories for thirty examples were constrained by high resolution LiDAR elevation data (cases 1-30); for two meander-belt reaches of the Sacramento, interpretations by Greco and Alford (2003) were referred to (cases 31-32); two meander-belt segments of the Mississippi have been modeled integrating observations from satellite images with channel trajectories digitized by Wiman et al. (2021) based on paleochannels mapped originally by Fisk (1944) (cases 33-34). The chosen examples have been selected to cover a range of accretion styles and variable degrees of channel-belt maturity. All meander-belt examples have been normalized by scaling them to the same channel width, to enable comparisons of quantities that depend on river-system size in nature (namely the time recorded by a channel-belt of a given extent). The modeling outputs are then applied to compare how preservation of meander-belt deposits varies over different temporal and spatial scales, for different hierarchies of sedimentary products (from smaller-scale pairs of accretion packages, to sets of multiple depositional packages associated with a state of meander transformation, to larger-scale channel belts).

The Point-Bar Sedimentary Architecture Numerical Deduction, PB-SAND (Yan et al., 2017), is used to model the planform evolution seen in the chosen meander belts based on the channel trajectories defined for each example. Additional centerlines that represent the planform expression of accretion surfaces, and which reflect the position of the river course between the input trajectories, are generated by linear interpolation. The number of accretion packages between two input trajectories were specified based on the planform spacing of scroll-bar morphologies observed in high-resolution LiDAR images. The average spacing across all the models (0.18 times channel widths) is consistent with that reported in the literature for the Mississippi River (Strick et al., 2018) (Figure S2). Meander-belt accretion is simulated in steps during which both erosion and deposition of accretion packages can take place, whereas no erosion is modeled within each accretion package bounded by two consecutive accretions surfaces. Although PB-SAND can be applied to model the 3D sedimentary architecture and facies distributions of meander belts and their accumulated deposits arising from different morphodynamics processes (Yan et al., 2017, 2020), in view of the scope of this research, only 2D planform evolutions of meander belts are reconstructed in this work.

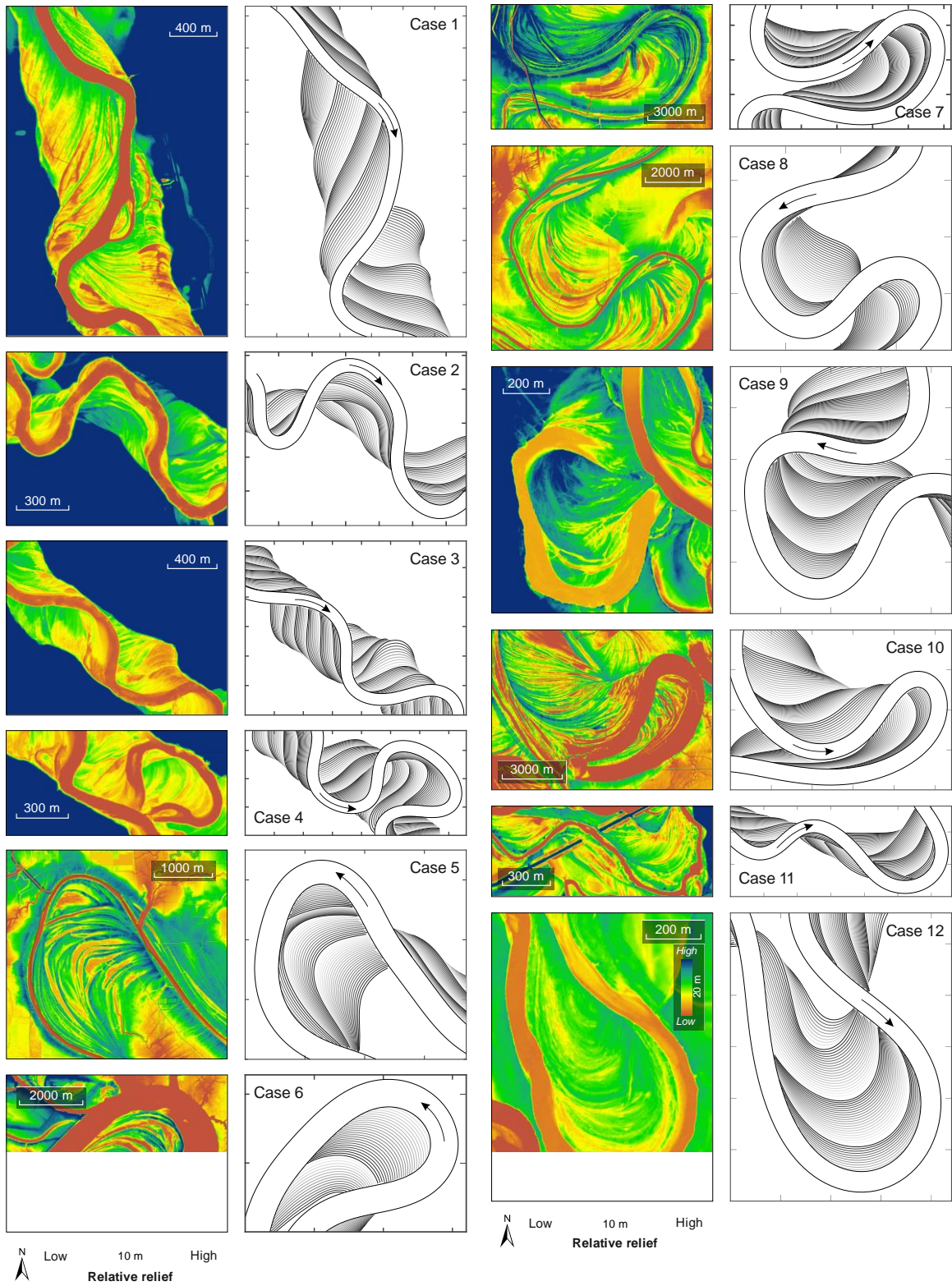


Figure S1. Thirty-four meander-belt cases portraying the planforms modeled using PB-SAND and corresponding model outputs. Arrows show flow direction.

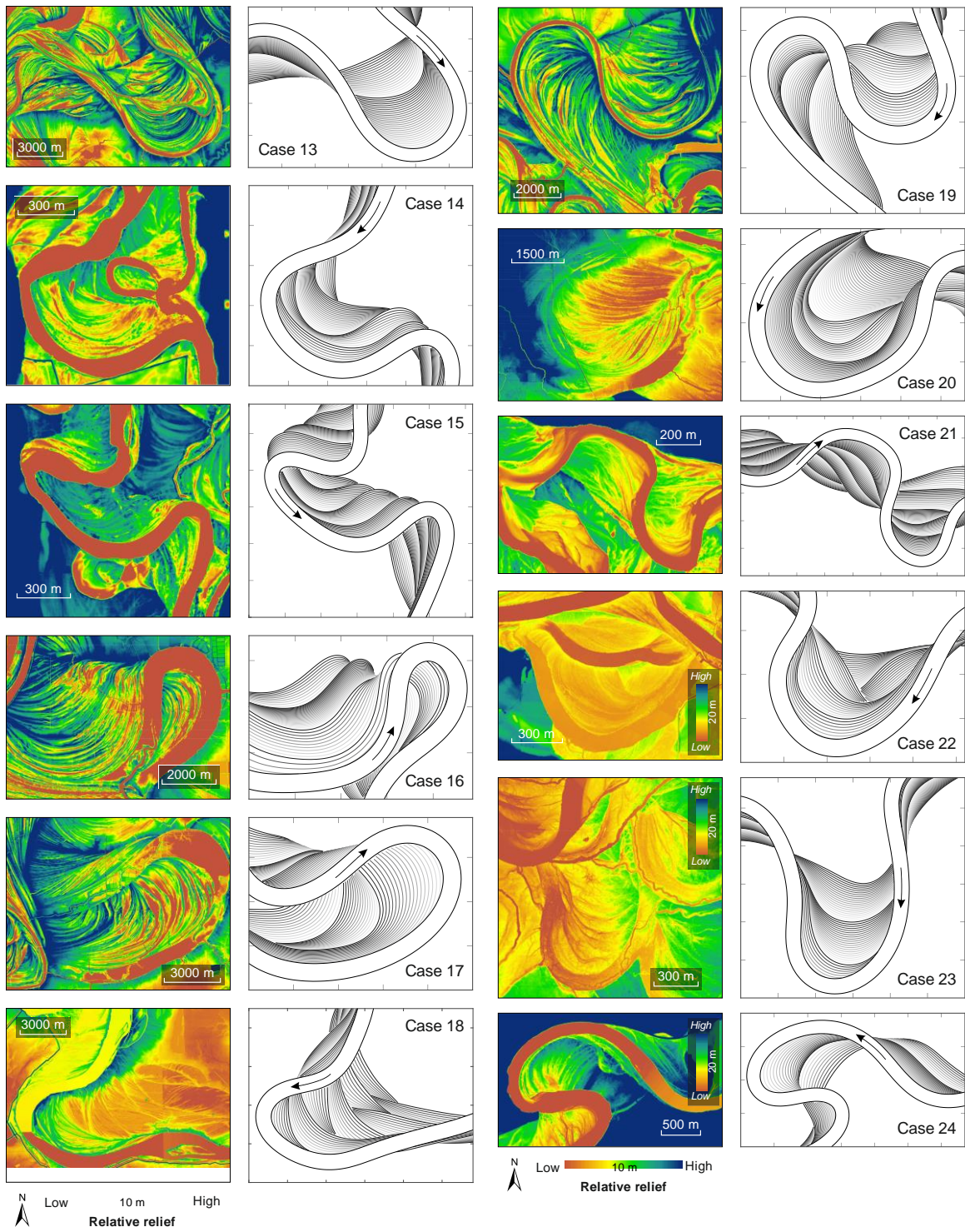


Figure S1. Continued.

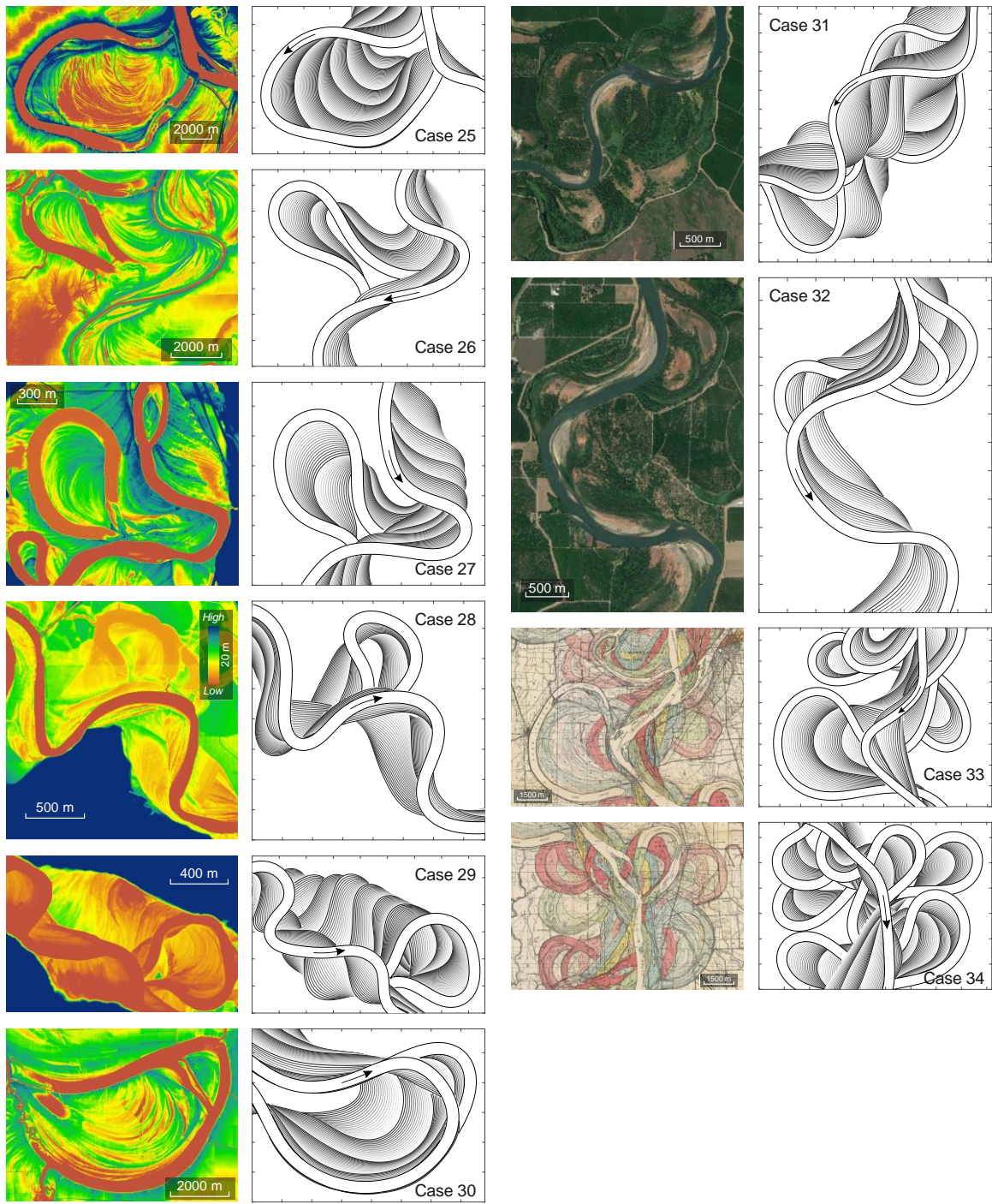


Figure S1. Continued.

Planform ID	Coordinates		Location
1	119° 24' 56" W	48° 50' 00" N	Okanogan, USA
2	29° 28' 07" E	66° 20' 37" N	Oulanka, Finland
3	29° 33' 21" E	66° 18' 45" N	Oulanka, Finland
4	29° 30' 36" E	66° 19' 54" N	Oulanka, Finland
5	119° 25' 11" W	48° 51' 31" N	Okanogan, USA
6	91° 32' 36" W	31° 53' 57" N	Mississippi, USA
7	91° 53' 16" W	30° 48' 53" N	Mississippi, USA
8	91° 21' 29" W	32° 18' 37" N	Mississippi, USA
9	119° 42' 43" W	48° 57' 43" N	Okanogan, USA
10	91° 32' 18" W	31° 46' 13" N	Mississippi, USA
11	119° 39' 24" W	48° 55' 40" N	Okanogan, USA
12	120° 06' 00" W	46° 15' 34" N	Yakima, USA
13	91° 27' 19" W	31° 51' 10" N	Mississippi, USA
14	91° 30' 06" W	30° 46' 21" N	Mississippi, USA
15	119° 26' 15" W	48° 54' 30" N	Okanogan, USA
16	91° 44' 45" W	31° 29' 31" N	Mississippi, USA
17	91° 38' 19" W	31° 38' 40" N	Mississippi, USA
18	120° 03' 53" W	46° 14' 42" N	Yakima, USA
19	91° 21' 50" W	32° 03' 30" N	Mississippi, USA
20	92° 02' 39" W	30° 55' 20" N	Mississippi, USA
21	119° 40' 28" W	48° 56' 47" N	Okanogan, USA
22	91° 36' 46" W	31° 33' 43" N	Mississippi, USA
23	121° 34' 19" W	48° 28' 42" N	Skagit, USA
24	121° 50' 24" W	48° 32' 05" N	Skagit, USA
25	91° 25' 20" W	30° 38' 50" N	Mississippi, USA
26	91° 22' 25" W	32° 21' 27" N	Mississippi, USA
27	119° 25' 13" W	48° 51' 33" N	Okanogan, USA
28	120° 04' 05" W	46° 14' 56" N	Yakima, USA
29	29° 35' 10" E	66° 18' 21" N	Oulanka, Finland
30	91° 13' 34" W	32° 27' 29" N	Mississippi, USA
31	121° 57' 42" W	39° 40' 55" N	Sacramento, USA
32	122° 00' 03" W	39° 30' 54" N	Sacramento, USA
33	91° 08' 46" W	33° 20' 26" N	Mississippi, USA
34	91° 05' 41" W	33° 13' 01" N	Mississippi, USA

Table S1. Location of thirty-four real-world meander-belt examples that display the same channel evolutions of the idealized models simulated in this work.

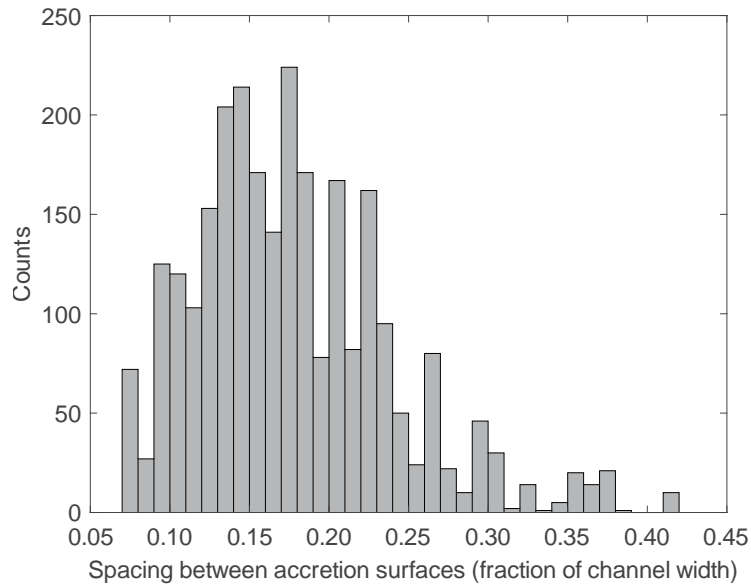


Figure S2. Distribution of the maximum spacing between accretion surfaces normalized by the channel width, from all 34 cases.

The 'preservation ratio' is the fraction of meander-belt deposits that are preserved over a given timescale, and is quantified as the ratio between the planform area covered by deposits accumulated over a certain length of time that are preserved at the end of that time window (area of net deposition) and the area over which the river has wandered over the same length of time (area of river migration) (Durkin et al., 2018). The preservation ratio is separately calculated for three hierarchies of architectural products:

- (i) pairs of accretion packages, whereby each package is contained between two consecutive accretion surfaces. Accretion packages can be regarded as analogous to flood-interflood units; however, they are modelled to have developed at a constant rhythm because accretion is simulated through linear interpolation between two input trajectories. Erosion within individual accretion packages is not simulated.
- (ii) sets of accretion packages bounded by two consecutive input trajectories, which represent portions of channel belts undergoing a certain style of meander transformations and are here termed 'stages' (stages contain between 5 and 40 accretion packages, 16 on average).
- (iii) meander-belt segments that are composed of multiple sets of accretion packages, each of which may be dominated by different styles of meander

transformations, and that record a variable number of bend cut-offs (from 0 to 6).

The time recorded in each accretion package is determined by the ratio between channel migration distance and channel migration rate. The channel migration distance was determined by the ratio of the area of river migration of each package to the average channel length of the two channel centerlines that define the package. The channel migration distance was then normalized with the channel width (arbitrary and of the same size across the 34 examples), as the 'normalized migration distance'. Values of average channel migration rate over each depositional package enclosed by two channel centerlines was determined based on three alternative assumptions of its relationship with the channel radius of curvature (Howard and Knutson, 1984; Hudson and Kesel, 2000; Nanson and Hickin, 1983; Sylvester et al., 2019). Three relationships between the normalized migration rate and the channel radius of curvature are considered, which yield three separate proxies for the temporal scale of river evolution: (i) channel migration rate remains constant for any value of channel radius of curvature; (ii) migration rate increases monotonically as the channel radius of curvature decreases (i.e. channel curvature increases); (iii) migration rate increases as the channel radius of curvature decreases towards 2.44 (cf. Howard and Knutson, 1984), and then decreases with increasing channel curvature (decreasing radius) for smaller radii of curvature. The second and third alternatives are determined based on relationships between channel radius of curvature and nominal migration rates that returned realistic relationships between actual channel migration rates and channel curvature in models by Howard and Knutson (1984, Figure 1a). The two relationships are presented in Figure 1d, in which the dimensionless arbitrary scale of Howard and Knutson (1984) is maintained. These relationships were not applied to extract migration rates for each node of a channel centerline (cf. Howard and Knutson, 1984), since each centerline represents a time step, wherefore relative rates of migration along each are given by the offset of these nodes relative to correlative nodes in neighboring centerline; instead, the relationships were used to extract dimensionless average migration rates for each package based on the average radius of curvature of two channel centerlines enclosing a sedimentary package. Across the entire set of channel trajectories (N = 3,952), the median value of the average radius of curvature of the centerlines is similar to the median of the local radii of curvature at the centerline nodes ('control points', Figure S3), and the two distributions are similarly skewed. The accretion time (t, dimensionless) was determined as the ratio of the normalized migration distance to the average migration rate:

$$t = \left(\frac{A}{LW} \right) / M$$

where A is the surface area of deposited package enclosed by two centerlines; L is the average length of two channel centerlines of a meander-belt segment; W is the channel width; M is the dimensionless average migration rate of the channel. M is equal to 1 for the first alternative, for which channel migration rate does not change with the average channel radius of curvature: in this case the migration distance is taken as a direct proxy

for time. The two time proxies associated with the second and third alternatives are also employed to compute meander-belt accretion rates for different hierarchies of architectural products: these accretion rates are defined as the ratios between preserved accretion distance divided by the time proxies.

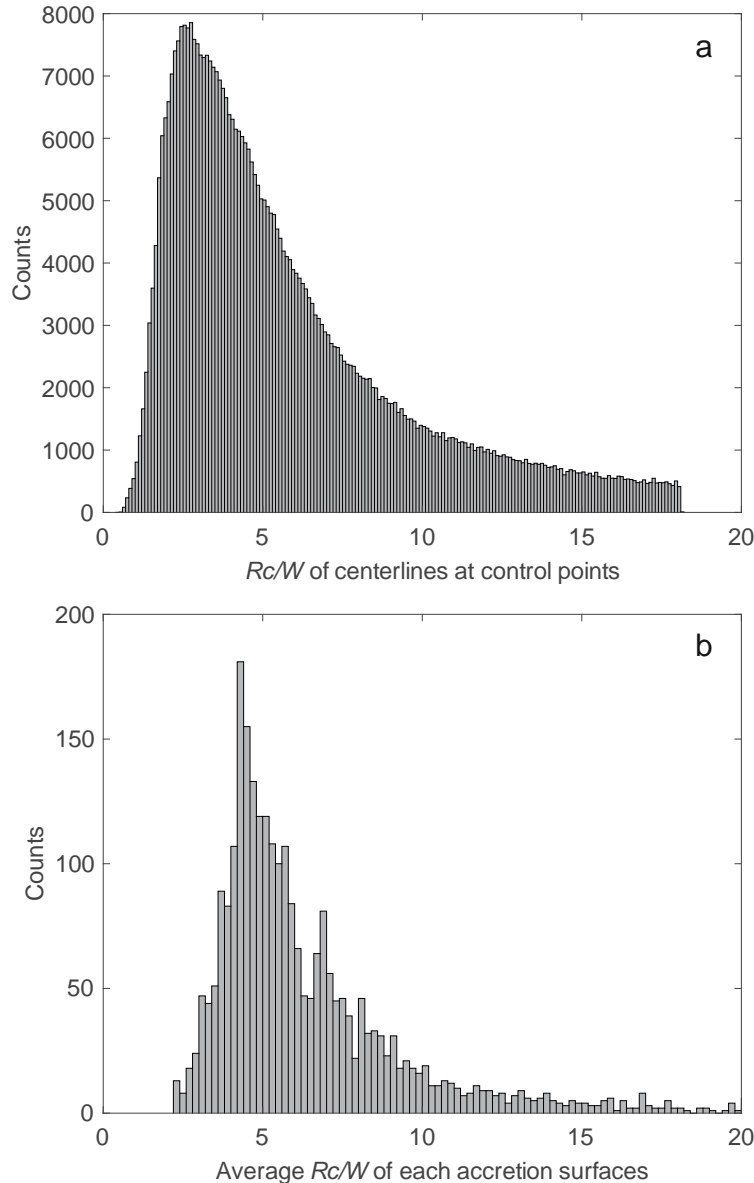


Figure S3. Distribution of the radius curvature of control points (A) and the average radius curvature of each accretion surface (B), both of which are normalized by the channel width, from all 34 cases.

Planform characteristics of each hierarchy of architectural products were analyzed including mean sinuosity, meander rotation, circular variance of channel orientation, and migration angle (Figure S4). The channel sinuosity is calculated as the ratio between the streamwise length and the straight distance between the two end points of each

modeled channel trajectory (Friend and Sinha, 1993). The channel sinuosity is further characterized by the circular variance of channel orientation, based on the downstream direction of pairs of consecutive control points (vector nodes) along the channel centerline. The degree of rotation of each meander is defined as the change of direction of the meander apex (itself identified as the point of local maximum curvature between two channel inflection points) across two consecutive accretion packages. The migration angle of each accretion package is defined as the absolute angle between the direction of channel migration, approximated by the direction of shift of corresponding control points across two consecutive trajectories, and the circular mean of downstream channel direction used as an approximation of the channel-belt orientation.

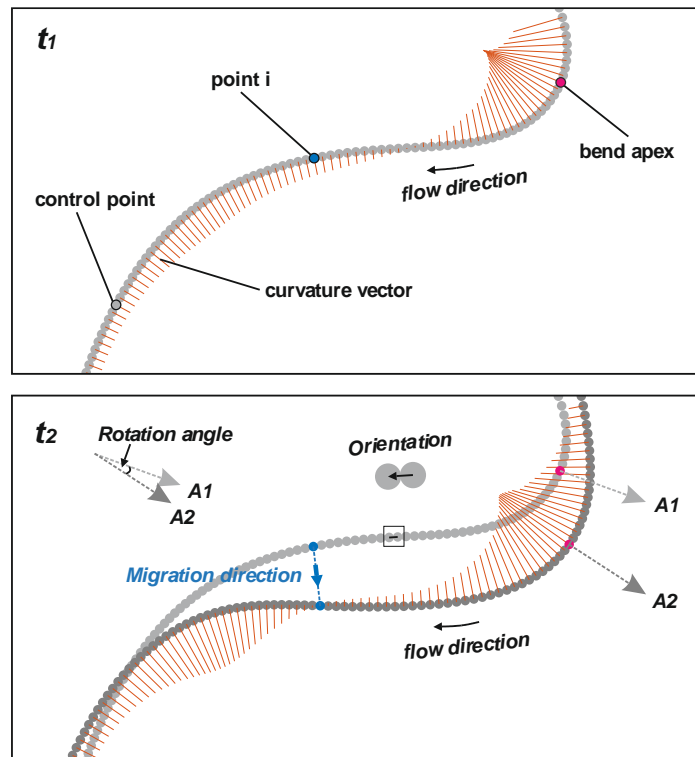


Figure S4. Schematic diagram showing how quantitative parameters of point-bar planform evolution are defined. Control points (vector nodes) of two consecutive channel centerlines at t_1 and t_2 are shown as gray spots. Each centerline has the same number of control points. The migration direction is calculated by the shift of each control point across consecutive centerlines. The channel orientation is estimated as a downstream-oriented vector connecting two consecutive control points along each centerline. The red lines denote the curvature vector of each control point, whereby a greater length indicates a sharper bend. The degree of apex rotation is the change in

migration direction seen between consecutive centerlines at the point of local maximum bend curvature (from Yan et al., 2020).

Limitations

The proposed approach is subject to several limitations. The assessment of sediment preservation of meander belts was undertaken considering planform areas as proxies for sediment volumes (Durkin et al., 2018). These volumetric estimations do not account for changes in meander-belt thickness in relation to streamwise variations in channel bathymetry (e.g., across meander pools and riffle zones, Yan et al., 2020). Furthermore, preservation of the lowermost portion of point-bar deposits caused by streambed aggradation is ignored in this particular study. Other possible limitations exist that are associated with necessary simplifications of the modeling approach. For example, the time embodied by accretion packages was calculated based on trajectories that are linearly interpolated so as to obtain accretion patterns that match with a realistic scroll-bar spacing (Strick et al., 2018); however, the spacing of scroll bars on point-bar surfaces may not accurately reflect the tempo of point-bar accretion, particularly in situations where erosional processes occur to shape scroll-bar morphologies (Mason and Mohrig, 2019; Nanson and Hickin, 1983). Another important simplification is made by computing the surface areas of accretion packages based on the migration of channel centerlines, rather than channel thalwegs, hence disregarding the fact that thalwegs will typically be offset relative to the centerlines, especially at pools located at meander apices. Examples of amalgamated meander-belt examples recording multiple episodes of neck or chute cutoffs, which cover the largest temporal scales considered, were modeled based on channel trajectories that are partly extracted from historical maps, which have lower temporal resolution than remote-sensing datasets.

References

- Durkin, P. R., Hubbard, S. M., Holbrook, J., & Boyd, R. (2018). Evolution of fluvial meander-belt deposits and implications for the completeness of the stratigraphic record. *GSA Bulletin*, 130(5-6), 721-739. <https://doi.org/10.1130/B31699.1>
- Fisk, H. N. (1944). *Geological investigation of the alluvial valley of the lower Mississippi River*. U.S. Department of the Army, Mississippi River Commission.
- Friend, P. F., & Sinha, R. (1993). Braiding and meandering parameters. In J. R. Best, & C. S. Bristow (Eds.), *Braided Rivers*, Geological Society, London, *Special Publications 75*, 105-111. m
- Hudson, P. F., & Kesel, R. H. (2000). Channel migration and meander-bend curvature in the lower Mississippi River prior to major human modification. *Geology*, 28(6), 531-534. [https://doi.org/10.1130/0091-7613\(2000\)28<531:CMAMCI>2.0.CO;2](https://doi.org/10.1130/0091-7613(2000)28<531:CMAMCI>2.0.CO;2)
- Mason, J., & Mohrig, D. (2019). Scroll bars are inner bank levees along meandering river bends. *Earth Surface Processes and Landforms*, 44(13), 2649-2659. <https://doi.org/10.1002/esp.4690>

- Nanson, G. C., & Hickin, E. J. (1983). Channel Migration and Incision on the Beatton River. *Journal of Hydraulic Engineering*, 109(3), 327-337.
[https://doi.org/10.1061/\(ASCE\)0733-9429\(1983\)109:3\(327\)](https://doi.org/10.1061/(ASCE)0733-9429(1983)109:3(327))
- Strick, R. J. P., Ashworth, P. J., Awcock, G., & Lewin, J. (2018). Morphology and spacing of river meander scrolls. *Geomorphology*, 310, 57-68.
<https://doi.org/10.1016/j.geomorph.2018.03.005>
- Sylvester, Z., Durkin, P., & Covault, J. A. (2019). High curvatures drive river meandering. *Geology*, 47(3), 263-266. <https://doi.org/10.1130/G45608.1>
- Wiman, C., Hamilton, B., Dee, S. G., & Muñoz, S. E. (2021). Reduced lower Mississippi River discharge during the Medieval era. *Geophysical Research Letters*, 48(3), e2020GL091182. <https://doi.org/10.1029/2020GL091182>
- Yan, N., Colombera, L., & Mountney, N. P. (2020). Controls on fluvial meander-belt thickness and sand distribution: Insights from forward stratigraphic modelling. *Sedimentology*. <https://doi.org/10.1111/sed.12830>
- Yan, N., Mountney, N. P., Colombera, L., & Dorrell, R. M. (2017). A 3D forward stratigraphic model of fluvial meander-bend evolution for prediction of point-bar lithofacies architecture. *Computers & Geosciences*, 105, 65-80.
<https://doi.org/10.1016/j.cageo.2017.04.012>

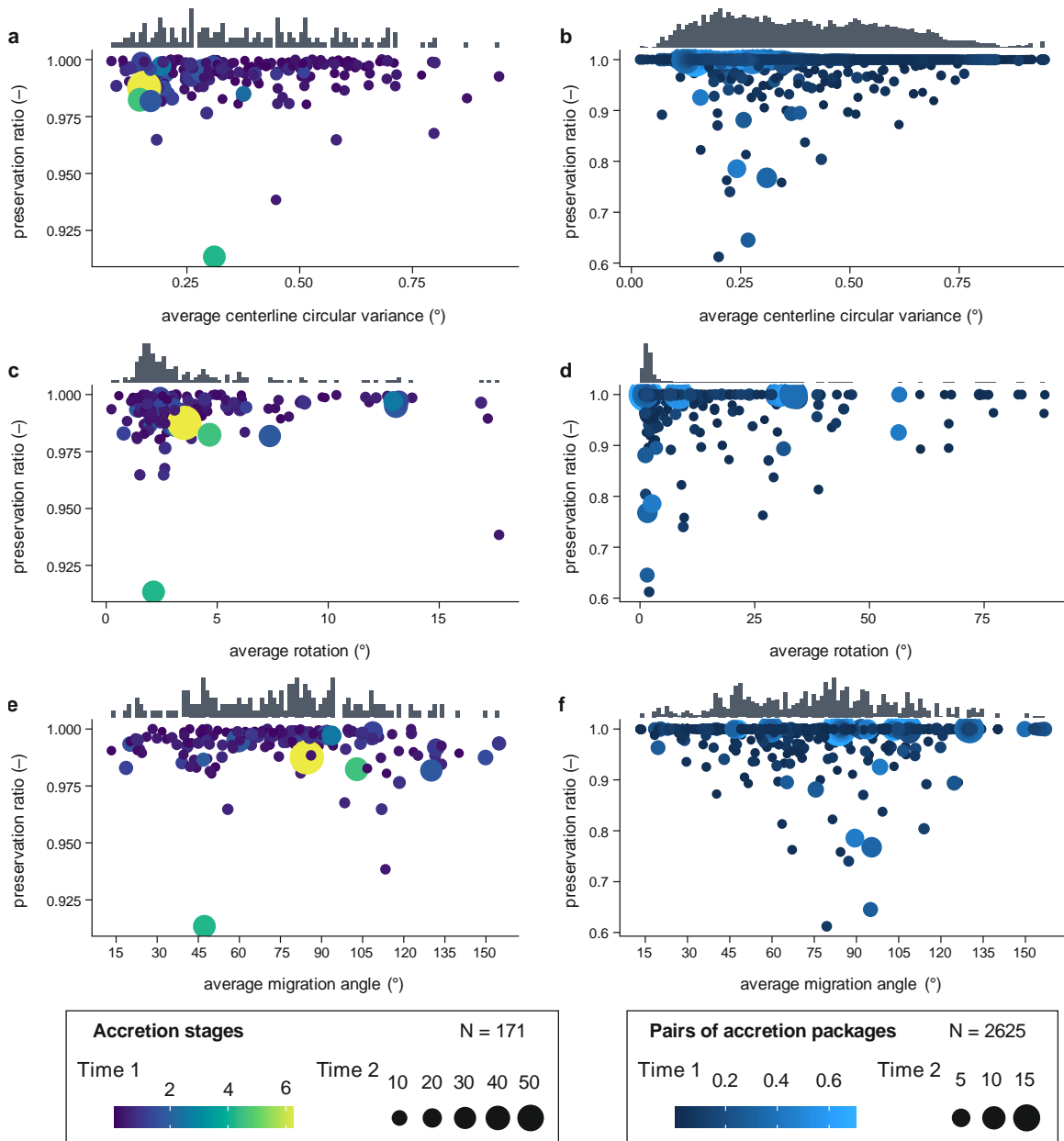


Figure S5. Relationships between the preservation ratio, planform characteristics and timescale of accretion stages and pairs of accretion packages, and associated distributions of planform metrics. The scatterplots show relationships between: average centerline circular variance and preservation ratio, for accretion stages (A) and pairs of packages (B); average meander-bend rotation and preservation ratio, for accretion stages (C) and pairs of packages (D); average migration angle (dominant accretion direction relative to channel orientation) and preservation ratio, for accretion stages (E) and pairs of packages (F).